Anisotropy of interband transitions in InAs quantum wires: An atomistic theory

Marco Califano and Alex Zunger
National Renewable Energy Laboratory, Golden, Colorado 80401, USA
(Received 4 March 2004; published 25 October 2004)

The electronic and optical properties of [001]-oriented free-standing InAs cylindrical quantum wires
(

growth,[9] the nanostructures are embedded in a lattice-matched fictitious wide-gap (~5.6 eV) material. This results in large band offsets and the absence of strain between matrix and wire. The atoms occupy therefore the ideal positions of a perfect zinc-blende bulk crystal.

Due to the large number of atoms involved, we solve Eq. (8) by using the *folded spectrum method*,[30,31] whereby it is possible to calculate exactly only selected eigenstates of the Schrödinger equation around an arbitrary reference energy e_{ref}. In this approach, Eq. (8) is replaced by

$$\left[-\frac{\hbar^2}{}\right.$$

IV. ATOMISTIC DESCRIPTION OF D_{2d} WIRES

The electronic structure of a nanostructure is calculated by solving the single-particle Schrödinger equation:

$$\left[-\frac{\hbar^2}{2m}\nabla^2 + V(\mathbf{r}) \right] c_i(\mathbf{r}) = e_i c_i(\mathbf{r}), \tag{8}$$

where $V(\mathbf{r})$ is the potential and e_i the energy eigenvalues. In the effective mass approximation, m is taken as the *effective* mass, and $V=V_{\mathrm{ext}}(\mathbf{r})$ is an *external* potential defining the geometric confinement of the nanostructure. We use a different approach, where $m=m_0$ is the actual (bare) electron mass and the microscopic pseudopotential of the system $V_{\mathrm{ps}}(\mathbf{r})$ is obtained as a superposition of screened atomic potentials,

$$V_{\mathrm{ps}}(\mathbf{r}) = \sum_{i,a} v_a(\mathbf{r} - \mathbf{R}_{i,a}), \tag{9}$$

where $v_a(\mathbf{r}-\mathbf{R}_{i,a})$ is the atomic potential for an atom of type a located at the position $\mathbf{R}_{i,a}$. The atomic pseudopotentials are derived from the bulk LDA screened pseudopotential and fitted to reproduce the measured InAs bulk transition energies, deformation potentials and effective masses.[29] The total potential is then expressed as

$$V(\mathbf{r}) = V_{\mathrm{ps}}(\mathbf{r}) + V_{\mathrm{nl}}, \tag{10}$$

where V_{nl} accounts for the nonlocal part of the potential and includes the SO coupling. In this atomistic approach Eq. (9) we set up the zinc-blende geometry of the system (nanostructure plus its surrounding matrix) in a supercell with periodic boundary conditions. The supercell size is chosen so as to minimize any interaction between neighboring nanostructures. This is obtained by increasing the supercell size until the calculated electron ground state energy does not change to within 1 meV (the hole energies converge much faster than the electron energies). We model LCG grown wires as free-standing, unstrained systems. In order to simulate the effect of an oxide coating, that is often present after the wire

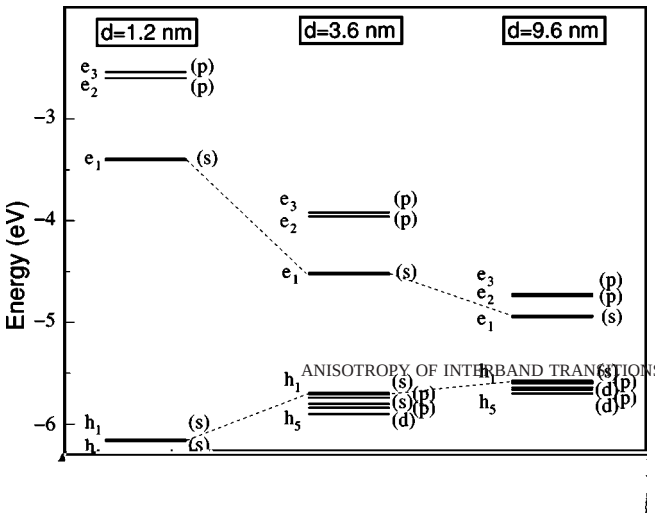

FIG. 1. Schematics of the calculated single-particle energy levels (labeled with their main angular momentum component) for 3 InAs D_{2d} cylindrical wires with sizes $d=1.2$, 3.6, 9.6 nm, respectively. The dashed lines connect, respectively, CBM and VBM in the different wires. Only a few states are shown that were used in the calculations of the optical properties.

with their main angular momentum component, relative to 3 InAs wire sizes: the thinnest, $d=1.2$ nm, the thickest, $d=9.6$ nm, and an intermediate size, $d=3.6$ nm. We see that the energy gap and the energy splitting between the subbands decreases with increasing wire diameter, owing to the decreased size confinement effect. As we will see, this feature is one of the causes of the different temperature behavior of the degree of linear polarization with different wire size.

B. Calculated polarizations and the role of dielectric mismatch

Figures 2 and 3 show the dipole matrix elements squared $|M|^2$ and the relative degree of linear polarization, for the $h_i \rightarrow e_j$ ($i=1,\ldots,6$ and $j=1,2,3$) transitions with light polarized along the wire axis (z-polarized) and perpendicular to it (x-polarized). The x- and z-polarized matrix elements relative to the same transition are offset for clarity. The degree of linear polarization shown was calculated from Eq. (6) considering only the anisotropy of the matrix elements but not the dielectric constant discontinuity between wire and surrounding material (i.e., $d=1$). Indeed $d \approx 1$ in a wire covered by an oxide, where the two materials have similar dielectric constants. In the case of a free standing wire in vacuum ($\varepsilon_{out}=1$), because of the small value of d in Eq. (6), the anisotropy due to the dielectric constant discontinuity dominates over the contribution due to the matrix element anisotropy. Using our calculated matrix elements and the values of $\varepsilon_{in}=14.6$ for the InAs dielectric constant and $\varepsilon_{out}=1$, we find that the degree of linear polarization of the fundamental transition $h_1 \rightarrow e_1$ assumes values . 99% for all wire diameters considered. On the other hand, if we assume isotropic matrix elements ($M^{\perp}=M^{\parallel}$) in Eq. (6), we obtain for the same systems the value of 96.8%. Therefore we find that, for a wire in vacuum, the matrix element anisotropy contributes by less than 3% to the total anisotropy.

C. Symmetry considerations

Table II summarizes the irreducible representations of the first 3 conduction and 5 valence subbands in $C_{\infty v}$,[19] D_{2d} and C_{4v} (Ref. 28) wires with similar sizes. In a $C_{\infty v}$ wire the lowest conduction subband $C^{(+)}(0)$ has even parity and is singly degenerate (excluding spin), whereas the next sub-

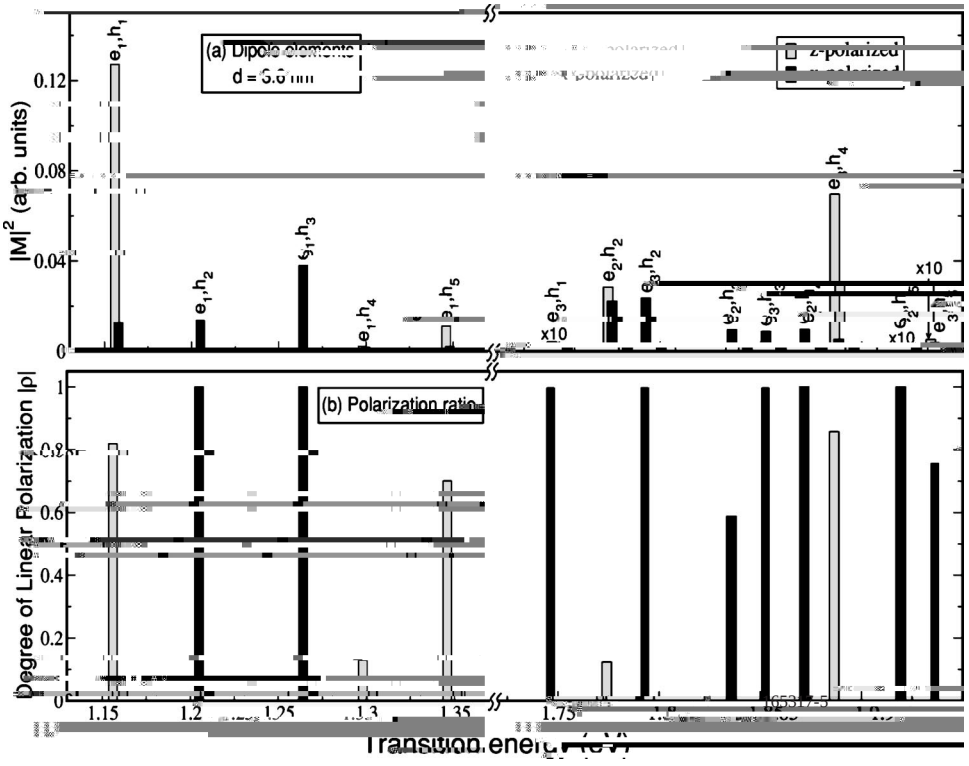

FIG. 2. (a) Matrix elements squared and (b) degree of linear polarization for the interband transitions $h_i \rightarrow e_j$ ($i=1,\ldots,5$, $j=1,2,3$), as a function of the transition energy for the $d=3.6$ nm InAs wire.

band $C^{(-)}(1)$

the different angular momentum composition of the subbands, which is manifested in different l-forbidden transitions; (ii) the fact that in continuous wires the subbands always have pure l character, as opposed to atomistic wires where, as discussed in Sec. III, each subband receives contributions from different angular momentum components. The angular momentum selection rule is therefore relaxed in D_{2d} wires and formally forbidden transitions may become weakly allowed. We find that this mixing of l character in the wave functions of D_{2d} wires increases with decreasing wire diameter (i.e., with increasing confinement) and with increasing subband position (i.e., h_5 and e_3 are more mixed than h_1 and e_1). This is reflected in the decrease, with increasing wire diameter, of the magnitude of the optical matrix elements relative to the formally angular-momentum-forbidden transitions [compare Figs. 2(a) and 3(a)]. Furthermore the lower degree of angular momentum component mixing in e_2 compared to e_3 is shown in the fact that, although both conduction states have main p character (and h_1 main (Tabction5. 31III*(transitions))]5bw.05[1] (s2877 41

effects in actual 1D systems are due to substantial mixing between the four bulk Γ_{8v}- *and* the two Γ_{7v}-derived valence bands.

The next transition ($h_2 \rightarrow e_1$), is a $\Gamma_7 \rightarrow \Gamma_6$ transitions in both D_{2d} and C_{4v} wires and is therefore allowed to be polarized only perpendicular to the wire axis. The $h_2 \rightarrow e_1$ and the $h_4 \rightarrow e_1$ transitions are forbidden[19] in C_{4v} QWRs, due to the different parity of the electron and hole wave functions. As discussed above, these transitions would be formally (angular-momentum) forbidden in our D_{2d} wires as well. However, due to the nonzero $l=1$ component of e_1 we find that they are weakly allowed: the dipole matrix elements for these transitions decrease by over one order of magnitude with increasing wire diameter (i.e., with decreasing l mixing in e_1), from 2.4 nm to 9.6 nm (both becoming less than 1% of the value of the matrix element relative to the band gap transition in the $d=9.6$ nm wire). As the $h_3 \rightarrow e_1$ transition is only x-polarized in C_{4v} wires, the two lowest energy transitions have opposite polarizations in D_{2d}, C_{4v}, and C_{4v} wires. The fundamental transition is in fact polarized mainly along the wire axis while the next allowed transition has only x polarization in all symmetries. The $h_4 \rightarrow e_1$ transition, instead, being a transition between two Γ_6 subbands, can have both polarizations: however, in d . 4.8 nm D_{2d} structures, it is only polarized perpendicular to the wire. The polarization component parallel to the wire axis increases from zero[34] to a value which is larger than that of the perpendicular component, when the wire diameter decreases from 9.6 nm to 3.6 nm.

Temperature dependence: We find (Figs. 4 and 5) a stronger temperature dependence for $\rho(h_1 \rightarrow e_1)$ in thick wires: in a $d=9.6$ nm wire ρ decreases by 10% with a 300 K temperature increase, compared to a 0.25% decrease in a $d=1.2$ nm wire, for the same temperature variation. This size dependence of the polarization can be understood in terms of lateral confinement effects. Due to the quantum size effect, thin wires experience a stronger confinement than thicker wires, which means that they have a higher kinetic energy introduced by the confinement. As this kinetic energy is responsible for the mixing[20] of the valence bands at zone center, thin wires have also a stronger mixing and therefore a

tion, found in Fig. 3, is masked by the broadening of the fundamental transition in a $d = 9.6$ nm wire. In a $d = 1.2$ nm wire (

parameter $\gamma_2 = \gamma_3$) there is no polarization anisotropy in the plane normal to the wire axis in a $C_{\infty v}$ wire.[21] By including the effect of valence-band anisotropy, Yamaguchi and Usui[21] predicted a weak dependence on the wire orientation for the polarization along z, and a strong dependence for the polarization along two perpendicular directions x and y (both in-plane) for the fundamental transition in wires oriented in directions different than [001] and [111]. Furthermore, only for [001]- and [111]-oriented wires they found no in-plane anisotropy, i.e., $|M^x| = |M^y|$. For all other orientations the calculated dipole matrix elements along x and y were different.

Similarly, we find no in-plane anisotropy in the fundamental transition in D_{2d} wires. However, higher energy transitions show polarization anisotropy in the plane perpendicular to the wire axis. Figures 8 and 9 show the xy-plane ($\perp$ to the wire axis) anisotropy we find in the $h_4 \rightarrow e_1$ and $h_5 \rightarrow e_1$ transitions in D_{2d} QWRs, grown along the [001] direction, with $d \geq 6$ nm, where the matrix element along the [110] direction is different from that along the $[1\bar{1}0]$ direction. We see that the $h_4 \rightarrow e_1$ transition is prevalently [110]-polarized with only the $d = 9.6$ nm wire polarized along $[1\bar{1}0]$. The opposite is true for the $h_5 \rightarrow e_1$ transition, where the only size for which the transition is prevalently polarized along [110] is $d = 6$ nm. However the $d = 9.6$ nm wire is found mainly polarized along $[1\bar{1}0]$ and the $d = 6$ nm wire mainly along [110], in both transitions. In all other transitions considered we found no anisotropy in the xy plane.

VI. SUMMARY

In summary we applied an atomistic, empirical pseudopotential method to calculate optical transitions in free-standing, unstrained [001]-oriented cylindrical InAs quantum wires with diameters in the experimentally accessible range 10–100 Å. We found evidence of strong coupling of bulk Γ_{8v}- and bulk Γ_7

1958 (1997).
[15] F. Vouilloz, D. Y. Oberli, M.-A. Dupertuis, A. Gustafsson, F. Reinhardt, and E. Kapon, Phys. Rev. Lett. **78**, 1580 (1997).
[16] J. A. Brum and G. Bastard, Superlattices Microstruct. **4**, 443 (1988).
[17] P. C. Sercel and K. J. Vahala, Appl. Phys. Lett. **57**, 545 (1990).
[18] P. C. Sercel and K. J. Vahala, Phys. Rev. B **42**, 3690 (1990).
[19] P. C. Sercel and K. J. Vahala, Phys. Rev. B **44**, 5681 (1991).
[20] U. Bockelmann and G. Bastard, Phys. Rev. B **45**, 1688 (1992).
[21] A. A. Yamaguchi and A. Usui, J. Appl. Phys. **78**, 1361 (1995).
[22] P. Ils, Ch. Greus, A. Forchel, V. D. Kulakovskii, N. A. Gippius, and S. G. Tikhodeev, Phys. Rev. B **51**, 4272 (1995).
[23] E. A. Muljarov, E. A. Zhukov, V. S. Dneprovskii, and Y. Masumoto, Phys. Rev. B **62**, 7420 (2000).
[24] M. A. Dupertuis, E. Martinet, D. Y. Oberli, and E. Kapon, Europhys. Lett. **52**, 420 (2000).
[25] W. H. Zheng, J.-B. Xia, and K. W. Cheah, J. Phys.: Condens. Matter **9**, 5105 (1997).
[26] D. S. Citrin and Y.-C. Chang, J. Appl. Phys. **70**, 867 (1991).
[27] G. Bester, S. Nair, and A. Zunger, Phys. Rev. B **67**, 161306 (2003).
[28] D. S. Citrin and Y.-C. Chang, Phys. Rev. B **40**, 5507 (1989).
[29] L. W. Wang and A. Zunger, Phys. Rev. B **51**, 17398 (1995); H. Fu and A. Zunger, *ibid.* **56**, 1496 (1997).
[30] L. W. Wang and A. Zunger, J. Chem. Phys. **100**, 2394 (1994); J. Phys. Chem. **98**, 2158 (1994).
[31] L. W. Wang and A. Zunger, in *Semiconductor Nanoclusters*, edited by P. V. Kamat and D. Meisel (Elsevier, New York, 1996).
[32] L. D. Landau and E. M. Lifshitz, *Electrodynamics of Continuous Media* (Nauka, Moscow, 1992).
[33] G. F. Koster, J. O. Dimmock, R. G. Wheeler, and H. Slatz, *Properties of the Thirty-Two Point Groups* (MIT Press, Cambridge, 1966).
[34] We assume a matrix element $|M^{(i)}|^2$ $(i=\|, \perp)$ to be zero when its value is $\&10^{-4}|M^{\|}_{e1,h1}|^2$.